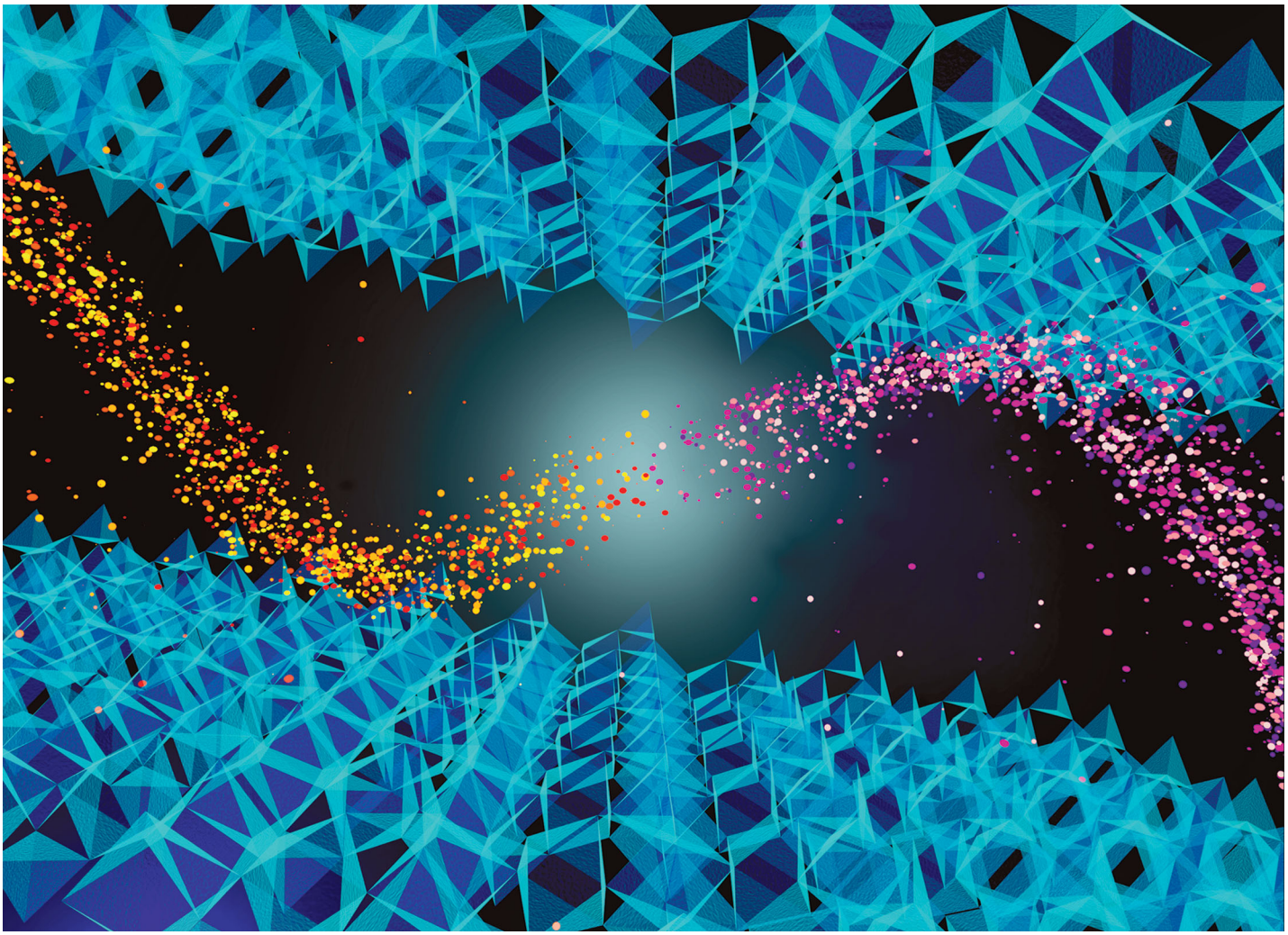

Highlighting research from Professor Lotsch's laboratory, Nanochemistry Department, Max Planck Institute for Solid State Research, Germany.

Customizing $H_3Sb_3P_2O_{14}$ nanosheet sensors by reversible vapor-phase amine intercalation

We report a facile, reversible two-step vapor phase amine intercalation protocol, which allows for the adaptive control of the structural and dielectric properties of $H_3Sb_3P_2O_{14}$ nanosheet-based thin films. This soft chemistry approach is expected to be generic and offers the possibility of creating novel structures with spatially dependent properties, thus adding a new patterning technique to the toolbox of soft lithography.

As featured in:

See Bettina V. Lotsch *et al.*, *Nanoscale Horiz.*, 2020, **5**, 74.

ROYAL SOCIETY OF CHEMISTRY

rsc.li/nanoscale-horizons

Registered charity number: 207890

Nanoscale Horizons

COMMUNICATION

View Article Online
View Journal | View Issue

Cite this: *Nanoscale Horiz.*, 2020, 5, 74

Received 3rd July 2019,
Accepted 19th September 2019

DOI: 10.1039/c9nh00434c

rsc.li/nanoscale-horizons

Customizing $H_3Sb_3P_2O_{14}$ nanosheet sensors by reversible vapor-phase amine intercalation†

Marie Däntl,[ab] Pirmin Ganter,[ab] Katalin Szendrei-Temesi,[ab] Alberto Jiménez-Solano [a] and Bettina V. Lotsch *[abc]

Harvesting the large property space of 2D materials and their molecular-level fine-tuning is of utmost importance for future applications such as miniaturized sensors for environmental monitoring or biomedical detection. Therefore, developing straightforward strategies for the reversible and gradual fine-tuning of nanosheet properties with soft chemical intercalation methods is in high demand. Herein we address this challenge by customizing the host–guest interactions of nanosheets based on the solid acid $H_3Sb_3P_2O_{14}$ by vapor-phase amine-intercalation with primary alkylamines. Fine-tuning of the structural and chemical properties of the intercalated nanosheets is achieved by applying a two-step, post-synthetic intercalation strategy *via* the vapor phase. The method allows for the gradual and reversible replacement of one amine type by another. Hence, fine-tuning of the *d*-spacing in the sub-Å regime is accomplished and offers exquisite control of the properties of the thin films such as refractive index, polarity, film thickness and sensitivity towards solvent vapors. Moreover, we employ amine replacement to pattern thin films by locally resolved amine intercalation and subsequent washing, leading to spatially dependent property profiles. This process thus adds a new vapor-phase, amine-based variant to the toolbox of soft lithography.

New concepts

Fine-tuning the (opto)electronic properties of nanosheet-based thin films post-synthetically and with high spatial resolution is required in order to create sophisticated devices – for example miniaturized sensors – more easily. So far, property tuning of 2D materials has been achieved for example *via* covalent or electrochemical intercalation and de-intercalation. However, these approaches are either non-reversible or require a complex setup. Therefore, straightforward strategies for fine-tuning the properties of nanosheet materials are in high demand. We herein report a facile, two-step amine intercalation protocol, which allows for the adaptive control of the structural and dielectric properties of amine intercalated $H_3Sb_3P_2O_{14}$ nanosheet thin films such as film thickness, polarity, sensitivity towards solvent vapors, and effective refractive index. This soft chemistry approach is expected to be generic and offers the possibility of creating novel structures with spatially dependent properties, thus adding a new patterning technique to the toolbox of soft lithography, based on reversible amine intercalation.

After the discovery of graphene, the interest in inorganic layered materials resurged, since like graphite, they can be exfoliated into two-dimensional (2D) nanosheets, which exhibit properties distinct from their bulk counterparts.[1–5] So far, exfoliation of a large variety of layered materials such as graphite,[6] transition metal dichalcogenides (TMD),[7] transition metal oxides (TMO),[8] layered double hydroxides (LDH),[9] Zintl phases[10] and MXenes[11] has been successful. Although these nanosheets exhibit many outstanding and diverse properties in their pristine form, tailoring and fine-tuning their properties in a rational manner for applications and processing is still challenging.[12–14]

As of now, there are five main strategies for modifying the physical and chemical properties of the nanosheets. These approaches include covalent functionalization,[12,15–17] intercalation and ion exchange,[18,19] morphology control,[20–23] nanoparticle decoration[24,25] and elemental substitution.[26,27] So far, post-synthetic tuning of the nanosheet properties over a broad range is only possible with covalent functionalization, electrochemical[28,29] and soft chemical intercalation, as well as ion exchange methods.[30–32] For instance, covalent modification has been utilized for functionalizing germanane nanosheets with organic groups to tailor their electronic structure.[15,33,34] Moreover, ion exchange reactions with different cations in graphene oxide (GO) membranes allow for precisely controlling the interlayer spacing, which leads to a change in the permeability of the membranes.[35] In addition, we demonstrated a vapor-phase amine intercalation strategy for modifying the swelling characteristics of $H_3Sb_3P_2O_{14}$ nanosheet-based thin films.[36] Apart from that, the gradual optoelectronic tunability

[a] *Max Planck Institute for Solid State Research, Heisenbergstrasse 1, 70569 Stuttgart, Germany. E-mail: b.lotsch@fkf.mpg.de*
[b] *Department of Chemistry, Ludwig-Maximilians-Universität (LMU), Butenandtstrasse 5-13, 81377 Munich, Germany*
[c] *E-conversion and Center for NanoScience, Schellingstrasse 4, 80799 Munich, Germany*

† Electronic supplementary information (ESI) available: Experimental section and supporting figures. See DOI: 10.1039/c9nh00434c

of $Ti_3C_2T_x$ (T = O, OH, F or other surface termination) MXene thin films was demonstrated by electrochemical intercalation.[37] While all of these methods are efficient in their present stage, only electrochemical intercalation and de-intercalation currently achieves a reversible and fine-tuned gradual modification, whereas a rather stepwise and non-reversible change in properties is observed for the other methods. In contrast to the other approaches, however, electrochemical intercalation requires a more complex experimental set-up.[18,37,38] Therefore, strategies for the straightforward, reversible and gradual fine-tuning of nanosheet properties with soft chemical intercalation methods are in high demand.

Inspired by intercalation studies of bulk materials[39] and ligand exchange reactions for nanocrystals[40] or nanoparticle assemblies,[41] here we present a comprehensive vapor-phase amine intercalation strategy for fine-tuning the properties of $H_3Sb_3P_2O_{14}$ nanosheet-based photonic thin films. We demonstrate that by using a two-step post-synthetic intercalation method a continuous and reversible fine-tuning of the *d*-spacing in the sub-Å regime is achieved, allowing for the exquisite control of the properties of the thin films. Hereby, the tunable properties include the optical properties such as the refractive index, the polarity, film thickness and sensitivity towards solvent vapors. Therefore, this intercalation approach stands out from covalent modification and electrochemical intercalation, as it combines an easy synthetic methodology with gradual and reversible tunability, which is a generic method that can be applied to a wide range of nanosheets.

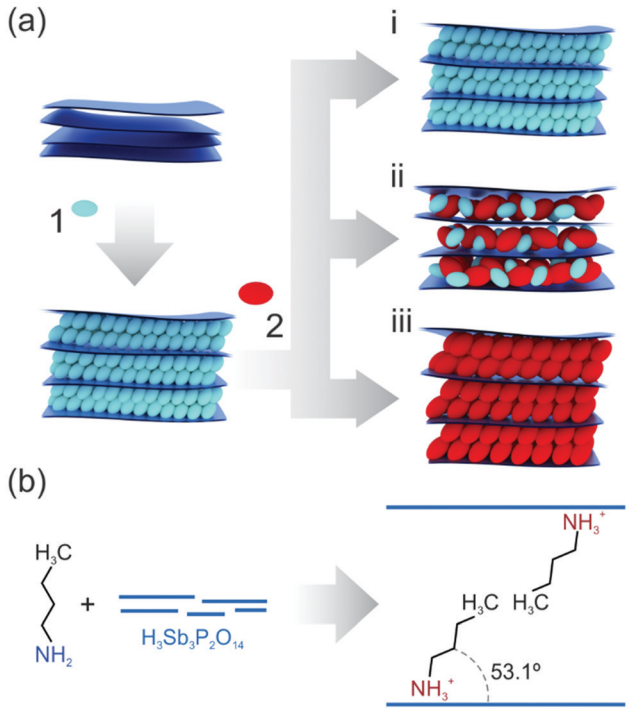

Fig. 1 (a) Schematic overview of the two-step intercalation of primary amines into nanosheet-based photonic thin films. (1) and (2) show the first and second intercalation step, respectively. (i), (ii) and (iii) highlight possible outcomes when exposing the amine intercalated thin film to the second, different amine vapor. (i): no exchange, (ii): co-intercalation, (ii): replacement. (b) Trapping of amines in the interlayer space through acid–base reaction and tilted bimolecular arrangement.[36]

Results and discussion

Fabry–Pérot photonic thin films producing structural colors due to thin film interference were chosen as an optical transducer since they enable the label-free colorimetric observation of intercalation processes in inherently colorless materials.[42] A scheme of the two-step intercalation protocol for tuning the properties of nanosheet-based photonic thin films is given in Fig. 1a. In the first step, $H_3Sb_3P_2O_{14}$ thin films were prepared by spin-coating and subsequently intercalated with primary alkylamines *via* the vapor phase.[36,43] Through the acid–base reaction of the amines with the interlayer protons of the solid acid $H_3Sb_3P_2O_{14}$, ammonium ions are formed and the amines are thus trapped in the interlayer space (Fig. 1b). Moreover, the amine-modified films exhibit a tilted bimolecular arrangement of the intercalants, and long-term stability of the amine intercalation was inferred by heating experiments (Fig. S1, ESI†). We find that the intercalated amines cannot be removed when heating the samples to 60 °C over a period of ten days. Note that in the following the nomenclature used for the intercalated amines refers to the number of carbon atoms in the alkyl chain (*e.g.* butylamine is named C4). In the second step, the primary alkylamine intercalated films were exposed to other primary alkylamines with various chain lengths. Hereby, different outcomes after an equilibration process can be imagined, including no change of the intercalated sample (i), a co-intercalation of two different amines (ii), or the complete replacement of the first intercalated amine by the second one (iii). The last two outcomes enable the versatile post-synthetic modification of the nanosheet-based thin films, as they allow for a gradual and reversible tailoring of the structural properties such as the interlayer distance, the optical properties, the polarity and, hence, wettability of the films. As a consequence, this makes a potentially vast property space accessible and at the same time allows for customizing the sensing response of a nanosheet sensor based on a single material.[44]

For the modification of the intercalated thin films in the second step, either longer or shorter amines than the ones already intercalated in step 1 can be used. These possibilities are referred to as "upward" (*e.g.* replacement of C2 by C4) and "downward" (*e.g.* replacement of C6 by C4) intercalation in the following. The differences in the alkyl chain lengths of the amines lead to a change in the interlayer distance. Hence, the upward and downward intercalation in $H_3Sb_3P_2O_{14}$ can be tracked optically (spectroscopically or by the naked eye) through the change in structural color, and by out-of-plane X-ray powder diffraction (XRPD). Our results immediately indicate that in the system studied here possibility (i) does not occur, since the interference color of the thin films invariably changes during the exposure to the second amine vapor, thus suggesting a change in the interlayer distances. When probed in Bragg–Brentano geometry, the XRPD patterns of the

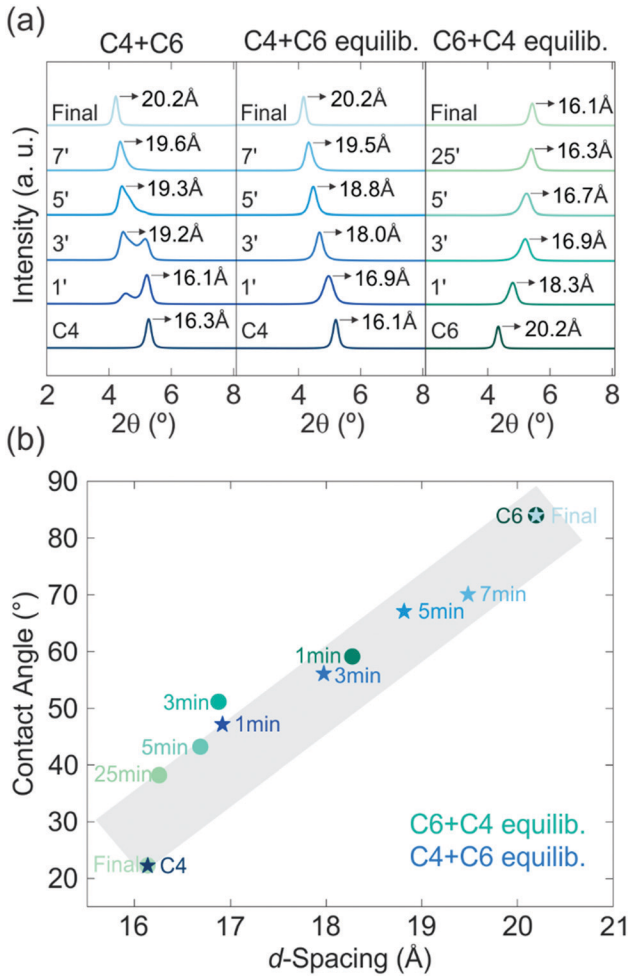

Fig. 2 Modification of primary alkylamine intercalated thin films with a second primary alkylamine in a two-step intercalation process allowing for sub-Å control of the interlayer space, *e.g.* from 16.9 to 16.7 Å, by changing the exposure time of a C6 intercalated sample to C4 from 3 to 5 minutes. (a) Out-of-plane XRPD patterns (Cu-$K_{\alpha 1}$) of upward and downward intercalation at different intercalation times in the range of 1 to 30 minutes. Patterns on the left were recorded directly after the intercalation (peak splitting), whereas the patterns in the middle and on the right were measured after the equilibration step (nearly uniform peaks). Upward intercalation results in an increase and downward intercalation leads to a decrease in the stacking distance. (b) Contact angle measurements of upward and downward intercalated samples in correlation with the *d*-spacing. The gray rectangle was inserted as a guide for the eye.

first step intercalated sample exhibit only 00*l* reflections due to the preferred orientation of the nanosheets parallel to the substrate.[45] Therefore, and considering the turbostratic disorder, the first reflection corresponds to the basal plane, *i.e.* the distance between the nanosheets. During the second intercalation step, the out-of-plane XRPD measurements in Fig. 2a (middle and right) reveal the gradual replacement of the first intercalated amine up to a complete exchange depending on the amine exposure time for the upward (C4 + C6) and downward (C6 + C4) intercalation. For these series of experiments, samples were taken from the intercalation chamber at a certain time (in the range of 1 to 30 minutes) during the second intercalation step, which either leads to a co-intercalation of both amines or a complete replacement of the first one (time dependence of Fig. 1b and c). Similar results were obtained for the C6 + C8 and C8 + C6 experiments (Fig. S2, ESI†). Note that these measurements were performed after a room temperature equilibration step, *i.e.* keeping the samples in a closed sample holder under ambient conditions for several days. When measuring the out-of-plane XRPD (Fig. 2a, left) of the sample directly after the second amine exposure a peak splitting is observed. The peak splitting strongly indicates non-uniform distribution and phase segregation of the amine guests within the thin film. During the equilibration step the amines diffuse through the film and mix, giving rise to uniformly intercalated interlayer spaces. As a consequence, the peak splitting in the XRPD patterns gradually vanishes leading to one single series of basal reflections, which do not change significantly over months. Therefore, a co-intercalation of both amines with a nearly uniform distribution is achieved.

Applying our two-step modification strategy, we are able to control the interlayer space continuously in the sub-Å regime, which is in contrast to previous nanosheet amine intercalation studies exhibiting a step-like change in *d*-spacing based on the amine chain length (Fig. 2b, ESI†).[36,46,47] The change in properties with modification of the *d*-spacing of the $H_3Sb_3P_2O_{14}$ thin films is underlined by contact angle measurements (Fig. 2b), as they show that the hydrophilicity of the C4 intercalated sample decreases continuously with exposure time towards C6 vapor due to the difference in the hydrophobicity of the used amines. The opposite behavior is observed for the exposure of the C6 intercalated sample towards C4, as expected. The continuous control of the *d*-spacing is highly important for fine-tuning the optical properties as well as the polarity of nanosheet-based thin films for different applications such as the development of chemo-selective sensors, optoelectronic devices, and membranes.[48,49] Specifically, through engineering the intergallery space at the sub-Å level very similar molecules with only subtle differences in size or polarity can exhibit significantly altered permeation rates, which enables possible applications in the field of membranes and sieving. For example, the fine control of the *d*-spacing influences the selectivity of physically confined GO (PCGO) membranes towards hydrated ions with similar sizes significantly due to their differences in size.[44] In addition, other important properties of nanosheets, such as the band gap, can also be influenced directly through the interlayer spacing.[50,51]

In order to demonstrate the scope of the amine exchange process and establish its generality, the experiments were carried out for various primary alkylamines with chain lengths ranging from C2–C12 (see Table S1, ESI†) and thus different hydrophilicity. The resulting stacking distances of the two-step amine exchanged samples are given in Fig. 3a. The *d*-values are all similar for each set of experiments, thus suggesting a complete exchange of the first intercalated amine in all cases. Taking into account the fact that co-intercalation results in altered *d*-values compared to the singly intercalated samples as discussed above, complete exchange can unequivocally be verified. The complete out-of-plane XRPD patterns of the experiment series

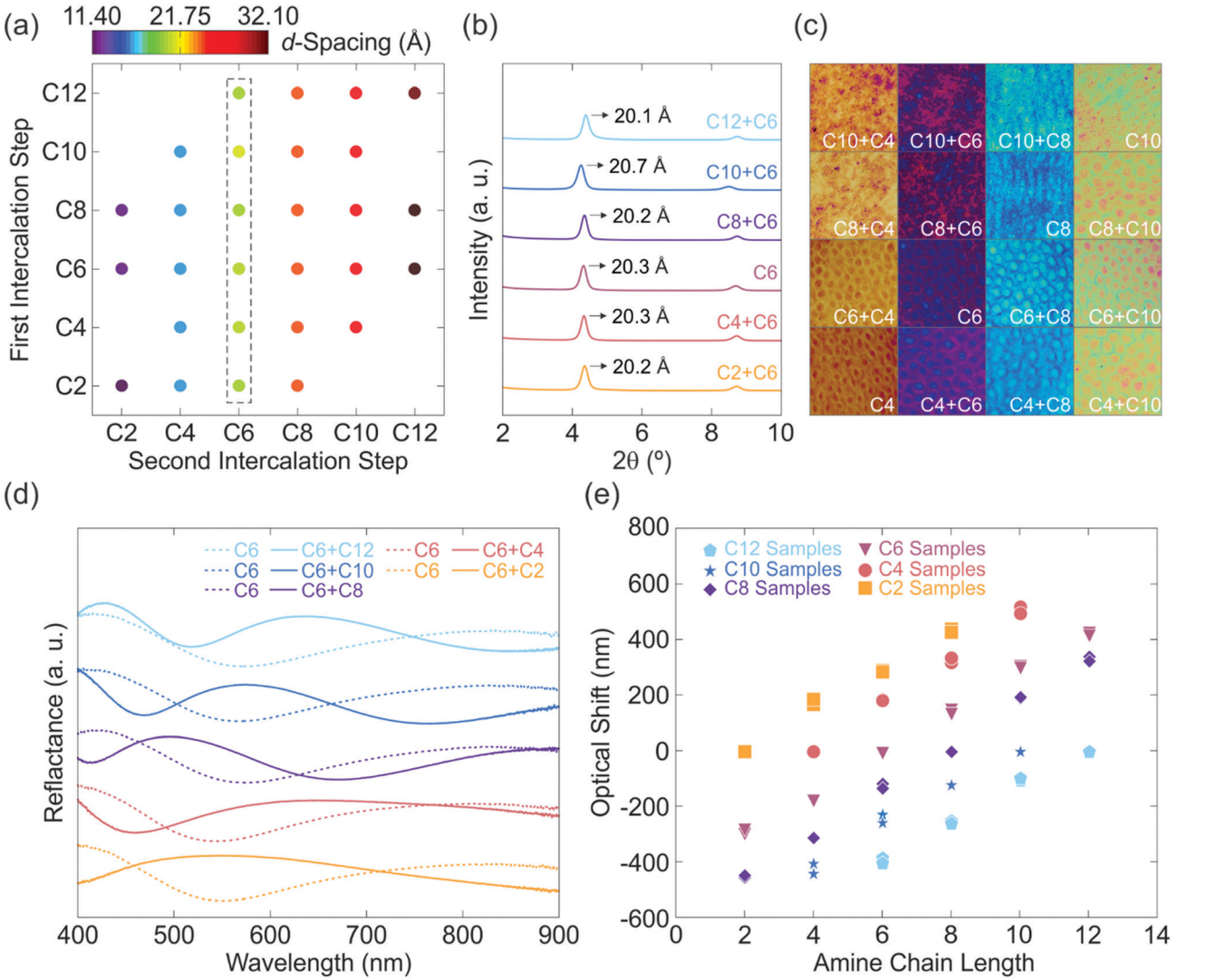

Fig. 3 (a) *d*-Values of all amine exchange experiments showing a complete exchange of the first intercalated amine after exposure to a second amine. (b) Detailed out-of-plane XRPD patterns (Cu-$K_{\alpha 1}$) for upward and downward intercalation of samples with C6. Second reflection observed at $\sim 8.7^{\circ}$ 2θ is the second order stacking reflection. (c) Comparison of some microscope images of singly and doubly intercalated $H_{3-x}(NH_3(CH_2)_{n-1}CH_3)_xSb_3P_2O_{14}$ thin films. (d) Reflectance spectra of the one-step C6 intercalated samples (dashed) and after the second intercalation step (solid lines). (e) Comparison of the relative optical shifts of all prepared thin films. Nomenclature: a certain color refers to samples intercalated with the same amine in the first intercalation step, *e.g.* all light blue pentagons represent samples, which contained dodecylamine in step one.

with C6 intercalated in the second step are given in Fig. 3b for upward as well as downward intercalated samples. It should be noted that the second reflection is the second order stacking reflection at $\sim 8.7^{\circ}$ 2θ. This implies a homogeneous exchange process. For out-of-plane XRPD patterns of the other experiment series see Fig. S3 (ESI†). Further confirmation of the complete exchange of the first intercalated amine is given by microscope images in combination with reflectance measurements (Fig. 3c–e). Fig. 3c shows microscope images of one- and two-step intercalated samples and indicates similar structural color for samples containing the same amine after the second intercalation step compared with the corresponding singly intercalated samples. Minor differences in color may arise from different film thicknesses before the intercalation due to the spin-coating process. The reflectance spectra of an upward as well as a downward intercalation starting from C6 are given in Fig. 3d (for other reflectance spectra see Fig. S4, ESI†) along with a comparison of the relative optical shifts of all conducted experiments in Fig. 3e. It can be observed that the optical shifts are linear and all show a similar slope for a certain amine. Note that the difference in color for each intercalated amine renders this system a versatile platform for applications in amine detection.

Complementary ellipsometry measurements (Fig. S5, ESI†) also evidence the complete replacement of the first intercalated amine. Furthermore, Raman measurements (Fig. S6, ESI†) support the previously discussed results, as the C–H vibrations of the amine chains offer a fingerprint to identify the intercalated species. With larger amine chain lengths, the observed peaks at 1200, 1300 (both νC–C or δC–H), 2900 and 3000 cm^{-1} (νCH_2 and νCH_3) become more pronounced and

the latter are slightly shifted towards smaller wavenumbers (see Fig. S6a, ESI†).

Since we could show that a partial up to a complete replacement of the first intercalated amine gradually takes place when exposing the sample to another amine vapor, this has important implications for customizing the interlayer space and, hence, sensor design, post-synthetically. The present experiments concentrated on showing the intercalation and exchange of primary alkylamines since there are many different ones with different hydrophilicity and therefore they allow a systematic study of the behavior. However, it is also possible to intercalate and exchange amines which are relevant in food spoilage control in the same manner. Very preliminary results for trimethylamine and 1,5-diaminopentane (both produced through microbial spoilage of fish and meat) are given in Fig. S7 (ESI†). The exchange of trimethylamine with C6 seems to take place on a similar timescale as observed for the primary alkylamines. Regarding the 1,5-diaminopentane the intercalation takes a lot longer (*ca.* 2 days) and therefore the exchange was not studied but should in principle be possible. The complete characterization of the intercalation and exchange of a large class of biologically relevant amines however, goes beyond the scope of this work.

For many applications cyclability of the intercalated sample is of prime importance and reversible intercalation would allow for versatile and repeated use. To demonstrate this possibility, cycling experiments were performed by intercalating the sample with C2 and subsequently replacing C2 with C8 and *vice versa*. Fig. 4a shows the position of the basal reflection obtained for the different intercalation states for up to five cycles, whereby the exposure to each amine leads to a complete replacement of the one intercalated before. This can be seen from the peak positions, where the stacking distances of all samples (Fig. 4a) are in good agreement with the ones of the singly C2 (11.5 Å) or C8 (24.4 Å) intercalated samples. Further, the complete replacement of the intercalated amines can also be tracked with the naked eye, which is shown in the insets in Fig. 4a. C2 samples exhibit a blue-yellow hue whereas the C8 samples show a purple-blue color. The two-step amine modification method is advantageous over other nanosheet modification methods such as covalent functionalization or nanoparticle decoration, for which a reversible and cyclable modification is notoriously difficult if not close to impossible to achieve. Moreover, our modification method stands out against electrochemical modification methods, as they commonly lack air stability and need an external power supply for cycling.[18,28]

Re-modification of the samples by intercalating and replacing amines with different properties can be used to build novel structures with arbitrary shapes and spatio-dependent, tailor-made properties. To demonstrate this concept, an entire

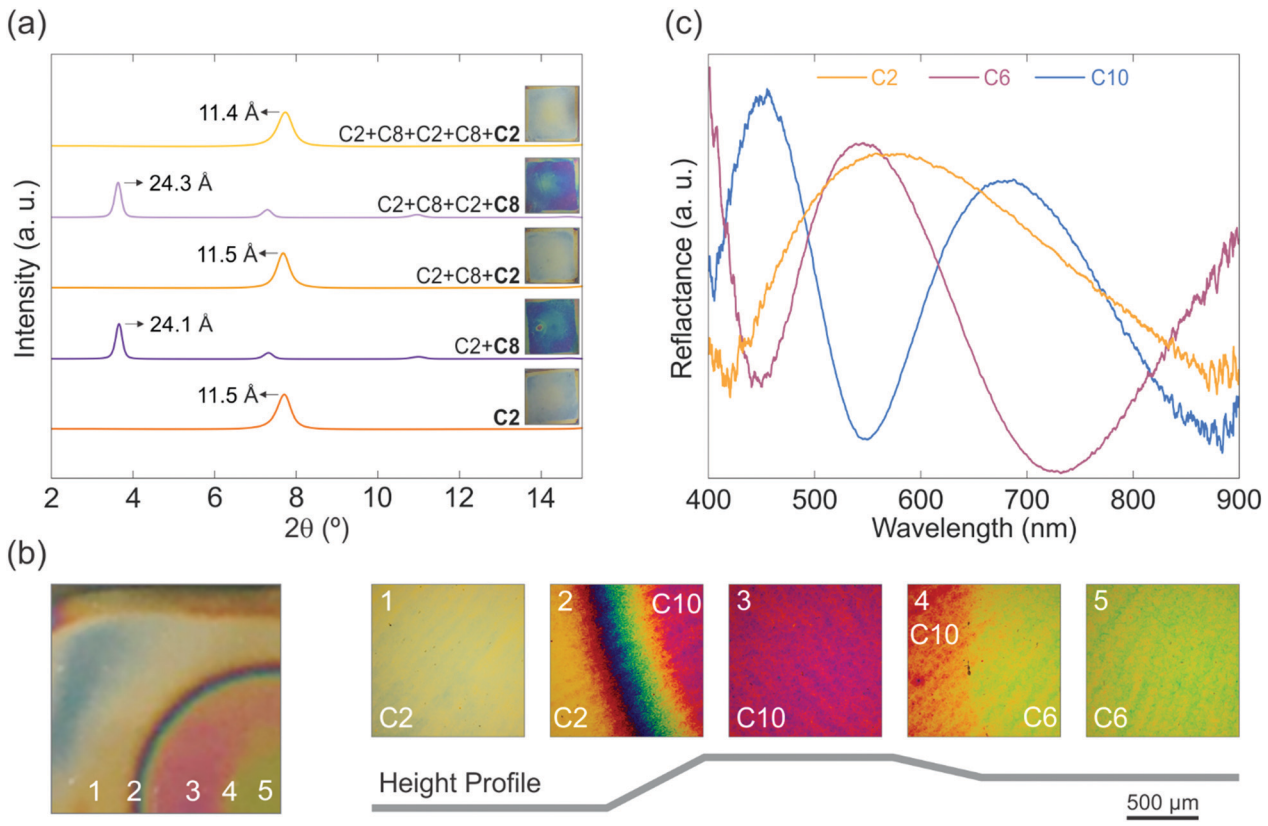

Fig. 4 (a) Out-of-plane XRPD patterns (Cu-$K_{\alpha 1}$) obtained for cycling experiments. A C2 intercalated sample was exposed to C8 and C2 in turn up to five times to show the cyclability and, hence, reversibility of the amine replacement. The insets of sample photographs show the sample color after each intercalation step. (b) Photograph of a three-step amine intercalated sample along with images of different regions of the sample and a schematic height profile for each part of the sample. The inset numbers indicate the corresponding region in the height profile. (c) Representative reflectance spectra for different parts of the sample.

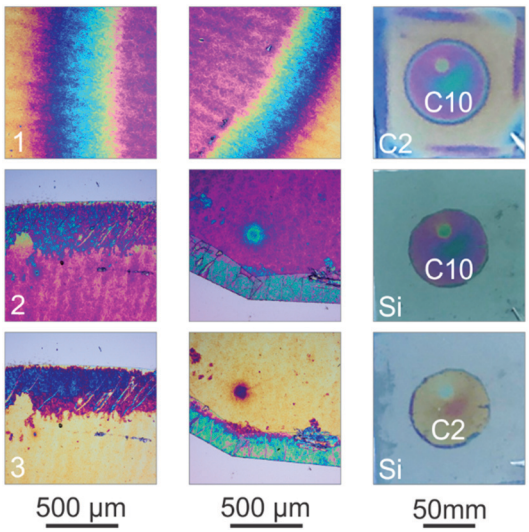

Fig. 5 Patterning through amine intercalation. Each row shows two images taken with an optical microscope (left and middle) along with a photograph of the sample (right). With the intermediate intercalation and washing step (2) a circular shape of C2 intercalated thin film (3) could be obtained.

wafer was intercalated with C2. Using a mask, a large circular part of the sample was subsequently replaced with C10. Finally, another smaller circular region in this circle was replaced with C6. A photograph of a three-step amine intercalated sample along with close-up images of different regions of the sample and a schematic height profile for different parts of the sample are depicted in Fig. 4b. The inset numbers indicate the corresponding region in the height profile. Furthermore, representative reflectance spectra are given for different parts of the sample (Fig. 4c). Due to the compactness and area-dependent functionality, these structures are good candidates for multi-purpose, miniaturized sensors.

Another example for an application of the amine replacement process is shown in Fig. 5. Since the spin-coating process during sample fabrication does not allow for patterning the deposited thin film, masks have to be applied during the intercalation step in order to obtain *e.g.* a circular amine intercalated thin film. To realize pattern formation, the C2-intercalated hydrophilic part of the sample given in Fig. 5(1), which has a circular part intercalated with hydrophobic C10, was removed by repeatedly washing the wafer with water yielding a hydrophobic circular thin film. However, this approach is only possible if the circular intercalated part contains a hydrophobic amine, which prevents this part from being washed away with polar solvents. If the desired pattern should be obtained with a hydrophilic amine at the end, the hydrophobic region can easily be turned into a hydrophilic one through re-modification by a short-chain amine such as C2 (Fig. 5(2)). Each row in Fig. 5 shows two microscope images along with a photograph of the sample (right). The differences in the color in the circular part arise from inhomogeneous thickness in the middle of the sample due to the spin-coating process. The modification could also be performed in the same manner using the pristine $H_3Sb_3P_2O_{14}$ thin film. In this case, however, the re-modification of a C2 intercalated thin film was chosen in order to compare the color with the obtained C2 modified circular thin film. The intercalation of more complex patterns, such as the letter "M", can also be achieved (see Fig. S8, ESI†), which enables the straightforward patterning of the amine modified thin film.

Changing the properties of surfaces in a spatially distinct manner through amine functionalization is currently also achieved with soft lithography methods, for example microcontact printing.[52,53] Soft lithography has the advantage of creating patterns with high spatial resolution down to about 30 nm with well-defined and controllable surface chemistry.[54] However, methods like microcontact printing are rather time-consuming in comparison to the amine intercalation strategy.[55] Therefore, the above-described patterning approach relying on amine-exchange and etching adds another easy and complementary method to the toolbox of soft lithography.

Conclusions

In summary, we showed that amine intercalated photonic thin films consisting of $H_3Sb_3P_2O_{14}$ nanosheets could easily be modified with other primary alkylamines with a straightforward, soft chemistry based reaction protocol *via* the vapor phase. We observe a continuous exchange of the first by the second amine until complete replacement is reached, which can be controlled through the exposure time (in the range of minutes) to the second amine vapor. Due to the continuous replacement of the first amine by a second amine, the interlayer spacing could be tailored on the sub-Å level and the polarity of the nanosheets was gradually fine-tuned over a broad range. The scope of the two-step amine modification strategy was verified by intercalating and replacing a large library of primary alkylamines. Furthermore, cycling experiments revealed that the modification is a reversible process, which allows for a versatile adaptive control of the materials' properties. This is a clear advantage compared to non-reversible covalent modification[12,17] of layered materials or sophisticated electrochemical control requiring external power supply and in most cases inert gas conditions.[18] Furthermore, patterning experiments indicate that the amine replacement method can be employed to create more complex structures coupled with area-resolved intercalation and etching.[36,56] Since the modification of other ionic and also non-ionic layered materials with amines has been studied frequently in the past,[36,57–60] the modification process developed in this work is most likely generic. Hence, it can be transferred to other nanosheet-based host materials displaying acid–base behavior and therefore opens up a new methodology for fine-tuning nanosheet properties for sensing applications and beyond. Other applications may lie in the field of membranes, in which the interlayer species takes the role of the gatekeeper controlling the selectivity through its shape (resulting *d*-spacing and properties, *e.g.* polarity).[61] More generally, the two-step amine intercalation approach may be utilized to fine-tune the mechanical[46,47] or (opto)electronic properties[62] of

nanosheet-based thin films post-synthetically and with high spatial resolution in order to create sophisticated devices more easily.[63]

Conflicts of interest

There are no conflicts to declare.

Acknowledgements

Financial support was granted by the Max Planck Society, the University of Munich (LMU) and the Cluster of Excellence e-conversion. The authors gratefully acknowledge Dimitra Chatzitheodoridou for providing her experience in thin film patterning and thank Armin Schulz for Raman spectroscopy, Christine Stefani for thin film X-ray diffraction measurements and James Borchert for contact angle measurements. A. J. S. gratefully acknowledges a postdoctoral scholarship from the Max Planck Society. Open Access funding provided by the Max Planck Society.

Notes and references

1 J. N. Coleman, M. Lotya, A. O'Neill, S. D. Bergin, P. J. King, U. Khan, K. Young, A. Gaucher, S. De, R. J. Smith, I. V. Shvets, S. K. Arora, G. Stanton, H.-Y. Kim, K. Lee, G. T. Kim, G. S. Duesberg, T. Hallam, J. J. Boland, J. J. Wang, J. F. Donegan, J. C. Grunlan, G. Moriarty, A. Shmeliov, R. J. Nicholls, J. M. Perkins, E. M. Grieveson, K. Theuwissen, D. W. McComb, P. D. Nellist and V. Nicolosi, *Science*, 2011, **331**, 568–571.
2 V. Nicolosi, M. Chhowalla, M. G. Kanatzidis, M. S. Strano and J. N. Coleman, *Science*, 2013, **340**, 1226419.
3 Y. Ebina, T. Sasaki and M. Watanabe, *Solid State Ionics*, 2002, **151**, 177–182.
4 T. Sasaki, *J. Ceram. Soc. Jpn.*, 2007, **115**, 9–16.
5 L. M. Liz-Marzán and M. Giersig, *Low-Dimensional Systems: Theory, Preparation, and Some Applications*, Springer, Berlin, 2003.
6 A. K. Geim and K. S. Novoselov, *Nat. Mater.*, 2007, **6**, 183–191.
7 J. A. Wilson and A. D. Yoffe, *Adv. Phys.*, 1969, **18**, 193–335.
8 K. Kalantar-zadeh, J. Z. Ou, T. Daeneke, A. Mitchell, T. Sasaki and M. S. Fuhrer, *Appl. Mater. Today*, 2016, **5**, 73–89.
9 R. Ma and T. Sasaki, *Adv. Mater.*, 2010, **22**, 5082–5104.
10 M. Q. Arguilla, J. Katoch, K. Krymowski, N. D. Cultrara, J. Xu, X. Xi, A. Hanks, S. Jiang, R. D. Ross, R. J. Koch, S. Ulstrup, A. Bostwick, C. Jozwiak, D. W. McComb, E. Rotenberg, J. Shan, W. Windl, R. K. Kawakami and J. E. Goldberger, *ACS Nano*, 2016, **10**, 9500–9508.
11 M. Naguib, V. N. Mochalin, M. W. Barsoum and Y. Gogotsi, *Adv. Mater.*, 2013, **26**, 992–1005.
12 W. L. B. Huey and J. E. Goldberger, *Chem. Soc. Rev.*, 2018, **47**, 6201–6223.
13 D. Sangian, Y. Ide, Y. Bando, E. Rowan Alan and Y. Yamauchi, *Small*, 2018, **14**, 1800551.
14 S. Bertolazzi, M. Gobbi, Y. Zhao, C. Backes and P. Samorì, *Chem. Soc. Rev.*, 2018, **47**, 6845–6888.
15 S. Jiang, M. Q. Arguilla, N. D. Cultrara and J. E. Goldberger, *Acc. Chem. Res.*, 2015, **48**, 144–151.
16 S. S. Chou, M. De, J. Kim, S. Byun, C. Dykstra, J. Yu, J. Huang and V. P. Dravid, *J. Am. Chem. Soc.*, 2013, **135**, 4584–4587.
17 D. Voiry, A. Goswami, R. Kappera, E. SilvaCecilia de Carvalho Castro, D. Kaplan, T. Fujita, M. Chen, T. Asefa and M. Chhowalla, *Nat. Chem.*, 2015, **7**, 45–49.
18 J. Wan, S. D. Lacey, J. Dai, W. Bao, M. S. Fuhrer and L. Hu, *Chem. Soc. Rev.*, 2016, **45**, 6742–6765.
19 M. Boota, M. Pasini, F. Galeotti, W. Porzio, M.-Q. Zhao, J. Halim and Y. Gogotsi, *Chem. Mater.*, 2017, **29**, 2731–2738.
20 M. Osada and T. Sasaki, *Dalton Trans.*, 2018, **47**, 2841–2851.
21 Z. Wang, J. Xuan, Z. Zhao, Q. Li and F. Geng, *ACS Nano*, 2017, **11**, 11559–11565.
22 C. Backes, B. M. Szydłowska, A. Harvey, S. Yuan, V. Vega-Mayoral, B. R. Davies, P.-l. Zhao, D. Hanlon, E. J. G. Santos, M. I. Katsnelson, W. J. Blau, C. Gadermaier and J. N. Coleman, *ACS Nano*, 2016, **10**, 1589–1601.
23 C. Backes, R. J. Smith, N. McEvoy, N. C. Berner, D. McCloskey, H. C. Nerl, A. O'Neill, P. J. King, T. Higgins, D. Hanlon, N. Scheuschner, J. Maultzsch, L. Houben, G. S. Duesberg, J. F. Donegan, V. Nicolosi and J. N. Coleman, *Nat. Commun.*, 2014, **5**, 4576.
24 D. Sarkar, X. Xie, J. Kang, H. Zhang, W. Liu, J. Navarrete, M. Moskovits and K. Banerjee, *Nano Lett.*, 2015, **15**, 2852–2862.
25 A. Jiménez-Solano, C. López-López, O. Sánchez-Sobrado, J. M. Luque, M. E. Calvo, C. Fernández-López, A. Sánchez-Iglesias, L. M. Liz-Marzán and H. Míguez, *Langmuir*, 2012, **28**, 9161–9167.
26 M. Osada, G. Takanashi, B.-W. Li, K. Akatsuka, Y. Ebina, K. Ono, H. Funakubo, K. Takada and T. Sasaki, *Adv. Funct. Mater.*, 2011, **21**, 3482–3487.
27 M. Osada and T. Sasaki, *Int. J. Appl. Ceram. Technol.*, 2012, **9**, 29–36.
28 J. S. Kang, M. Ke and Y. Hu, *Nano Lett.*, 2017, **17**, 1431–1438.
29 W. Bao, J. Wan, X. Han, X. Cai, H. Zhu, D. Kim, D. Ma, Y. Xu, J. N. Munday, H. D. Drew, M. S. Fuhrer and L. Hu, *Nat. Commun.*, 2014, **5**, 4224.
30 J. J. Cha, K. J. Koski, K. C. Y. Huang, K. X. Wang, W. Luo, D. Kong, Z. Yu, S. Fan, M. L. Brongersma and Y. Cui, *Nano Lett.*, 2013, **13**, 5913–5918.
31 J. Yao, K. J. Koski, W. Luo, J. J. Cha, L. Hu, D. Kong, V. K. Narasimhan, K. Huo and Y. Cui, *Nat. Commun.*, 2014, **5**, 5670.
32 K. Lu, Z. Hu, Z. Xiang, J. Ma, B. Song, J. Zhang and H. Ma, *Angew. Chem., Int. Ed.*, 2016, **55**, 10448–10452.
33 S. Jiang, K. Krymowski, T. Asel, M. Q. Arguilla, N. D. Cultrara, E. Yanchenko, X. Yang, L. J. Brillson, W. Windl and J. E. Goldberger, *Chem. Mater.*, 2016, **28**, 8071–8077.
34 S. Jiang, S. Butler, E. Bianco, O. D. Restrepo, W. Windl and J. E. Goldberger, *Nat. Commun.*, 2014, **5**, 3389.
35 L. Chen, G. Shi, J. Shen, B. Peng, B. Zhang, Y. Wang, F. Bian, J. Wang, D. Li, Z. Qian, G. Xu, G. Liu, J. Zeng, L. Zhang,

Y. Yang, G. Zhou, M. Wu, W. Jin, J. Li and H. Fang, *Nature*, 2017, **550**, 380–383.
36 P. Ganter, L. M. Schoop, M. Däntl and B. V. Lotsch, *Chem. Mater.*, 2018, **30**, 2557–2565.
37 K. Hantanasirisakul, M.-Q. Zhao, P. Urbankowski, J. Halim, B. Anasori, S. Kota, C. E. Ren, M. W. Barsoum and Y. Gogotsi, *Adv. Electron. Mater.*, 2016, **2**, 1600050.
38 S. Y. F. Zhao, G. A. Elbaz, D. K. Bediako, C. Yu, D. K. Efetov, Y. Guo, J. Ravichandran, K.-A. Min, S. Hong, T. Taniguchi, K. Watanabe, L. E. Brus, X. Roy and P. Kim, *Nano Lett.*, 2018, **18**, 460–466.
39 S. Jeong, D. Yoo, M. Ahn, P. Miró, T. Heine and J. Cheon, *Nat. Commun.*, 2015, **6**, 5763.
40 J. Buha and L. Manna, *Chem. Mater.*, 2017, **29**, 1419–1429.
41 D. Merg Andrea, Y. Zhou, M. Smith Ashley, E. Millstone Jill and L. Rosi Nathaniel, *ChemNanoMat*, 2017, **3**, 745–749.
42 P. Ganter and B. V. Lotsch, *Mol. Syst. Des. Eng.*, 2019, Advance Article.
43 K. Szendrei-Temesi, A. Jiménez-Solano and B. V. Lotsch, *Adv. Mater.*, 2018, **30**, 6289–6297.
44 J. Abraham, K. S. Vasu, C. D. Williams, K. Gopinadhan, Y. Su, C. T. Cherian, J. Dix, E. Prestat, S. J. Haigh, I. V. Grigorieva, P. Carbone, A. K. Geim and R. R. Nair, *Nat. Nanotechnol.*, 2017, **12**, 546–550.
45 P. Ganter, K. Szendrei and B. V. Lotsch, *Adv. Mater.*, 2016, **28**, 7436–7442.
46 S. Stankovich, D. A. Dikin, O. C. Compton, G. H. B. Dommett, R. S. Ruoff and S. T. Nguyen, *Chem. Mater.*, 2010, **22**, 4153–4157.
47 P. Gonzalez Rodriguez, H. Yuan, K. J. H. van den Nieuwenhuizen, W. Lette, D. J. Schipper and J. E. ten Elshof, *ACS Appl. Mater. Interfaces*, 2016, **8**, 28926–28934.
48 W.-S. Hung, C.-H. Tsou, M. De Guzman, Q.-F. An, Y.-L. Liu, Y.-M. Zhang, C.-C. Hu, K.-R. Lee and J.-Y. Lai, *Chem. Mater.*, 2014, **26**, 2983–2990.
49 K. H. Thebo, X. Qian, Q. Zhang, L. Chen, H.-M. Cheng and W. Ren, *Nat. Commun.*, 2018, **9**, 1486.
50 Q. Zhou, Q. Li, S. Yuan, Q. Chen and J. Wang, *Phys. Chem. Chem. Phys.*, 2017, **19**, 29232–29236.
51 Z. Hai and S. Zhuiykov, *Adv. Mater. Interfaces*, 2018, **5**, 1701385.
52 G. M. Whitesides, E. Ostuni, S. Takayama, X. Jiang and D. E. Ingber, *Annu. Rev. Biomed. Eng.*, 2001, **3**, 335–373.
53 R. G. Chapman, E. Ostuni, L. Yan and G. M. Whitesides, *Langmuir*, 2000, **16**, 6927–6936.
54 D. Qin, Y. Xia and G. M. Whitesides, *Nat. Protoc.*, 2010, **5**, 491–502.
55 G. M. Whitesides, J. K. Kriebel and B. T. Mayers, *Self-assembly and Nanostructured Materials*, Springer, Berlin, 2005.
56 P. Ganter and B. V. Lotsch, *Angew. Chem., Int. Ed.*, 2017, **56**, 8389–8392.
57 P. Ganter, L. M. Schoop and B. V. Lotsch, *Adv. Mater.*, 2017, **29**, 1604884.
58 R. M. Tindwa, D. K. Ellis, G.-Z. Peng and A. Clearfield, *J. Chem. Soc., Faraday Trans. 1*, 1985, **81**, 545–552.
59 Y. Wang, M. Nikolopoulou, E. Delahaye, C. Leuvrey, F. Leroux, P. Rabu and G. Rogez, *Chem. Sci.*, 2018, **9**, 7104–7114.
60 S. Ahmad, P. K. Kanaujia, W. Niu, J. J. Baumberg and G. Vijaya Prakash, *ACS Appl. Mater. Interfaces*, 2014, **6**, 10238–10247.
61 B. Mi, *Science*, 2014, **343**, 740–742.
62 R. Frisenda, A. J. Molina-Mendoza, T. Mueller, A. Castellanos-Gomez and H. S. J. van der Zant, *Chem. Soc. Rev.*, 2018, **47**, 3339–3358.
63 C. Wang, Q. He, U. Halim, Y. Liu, E. Zhu, Z. Lin, H. Xiao, X. Duan, Z. Feng, R. Cheng, N. O. Weiss, G. Ye, Y.-C. Huang, H. Wu, H.-C. Cheng, I. Shakir, L. Liao, X. Chen, W. A. Goddard Iii, Y. Huang and X. Duan, *Nature*, 2018, **555**, 231–236.